JOURNAL OF THERMOPHYSICS AND HEAT TRANSFER
Vol. 23, No. 2, April–June 2009

Modeling Thermal-Boundary-Layer Effect on Liquid–Vapor Interface Dynamics in Spray Cooling

R. Panneer Selvam,* Mita Sarkar,† and Suranjan Sarkar†
University of Arkansas, Fayetteville, Arkansas 72701
and
Rengasamy Ponnappan‡ and Kirk L. Yerkes§
U.S. Air Force Research Laboratory,
Wright–Patterson Air Force Base, Ohio 45433

DOI: 10.2514/1.34982

Spray cooling is a way of efficiently removing the heat from a hot surface and is considered for high-power systems such as advanced lasers. The heat transfer phenomenon in spray cooling is complex in nature because it occurs due to conduction, convection, and phase change. A brief review of the modeling of spray cooling is presented here. In the present work, the effect of thermal-boundary-layer thickness on liquid–vapor-interface dynamics and its influence on heat transfer in spray cooling is investigated through multiphase-flow modeling. The multiphase-flow modeling is done using the level-set method to identify the liquid–vapor interface. Some modifications to the incompressible Navier–Stokes equations to consider surface tension, viscosity, gravity, and phase change are discussed. The governing equations are solved using the finite difference method. Here, the droplet impact on a growing vapor bubble in a 44-μm-thick liquid film is taken as a benchmark problem to represent the spray cooling. The computed liquid–vapor-interface and temperature distributions are also visualized for better understanding of heat removal. In this study, the high-heat-transfer mechanism in spray cooling is explained with systematic illustrations.

Nomenclature

c_p	=	specific heat at constant pressure, J/kg · K
Fr	=	Froude number ($u_r/\sqrt{gl_r}$)
$\mathbf{g}$	=	gravity vector, m/s^2
H	=	step function
h	=	grid spacing, m
h_{fg}	=	latent heat of evaporation, J/kg
Ja	=	Jacob number ($cpl\Delta T/h_{fg}$)
k	=	thermal conductivity, W/m · K
l_r	=	characteristic length [$\sqrt{\sigma/g(\rho_l - \rho_v)}$], m
$\mathbf{m}$	=	mass flux vector, g/m^3/m^2 · s
m	=	mass flux
Nu	=	Nusselt number [$ql_r/(\Delta Tk_l)$]
n	=	surface normal
Pe	=	Peclet number ($\rho_l u_r l_r c_{pl}/k_l$)
Pr	=	Prandtl number ($c_{pl}\mu_l/k_l$)
p	=	pressure, Pa
q	=	heat flux, W/m^2
Re	=	Reynolds number ($\rho_l u_r l_r/\mu_l$)
T	=	temperature, K
T^*	=	dimensionless temperature [$(T - T_{\text{sat}})/(T_w - T_{\text{sat}})$]
t	=	time, s
t_r	=	characteristic time (l_r/u_r), s
$\mathbf{u}$	=	velocity vector (u, v), m/s
u	=	x-direction velocity, m/s
u_{int}	=	interface velocity, m/s
u_r	=	characteristic velocity ($\sqrt{gl_r}$), m/s
v	=	y-direction velocity, m/s
We	=	Weber number ($\rho_l u_r^2 l_r/\sigma$)
α	=	thermal diffusivity, m^2/s
ΔT	=	temperature difference ($T_w - T_{\text{sat}}$)
κ	=	interfacial curvature
μ	=	dynamic viscosity, N · s/m^2
ρ	=	density, g/m^3
σ	=	surface tension, N/m
φ	=	level-set function

Subscripts

int	=	interface
l, v	=	liquid, vapor
r	=	reference
sat	=	saturation
w	=	wall

Superscript

*	=	nondimensional quantity

I. Introduction

SPRAY cooling is a high-flux heat-removal technique considered for high-power systems. The spray cooling with phase change and droplet impact can achieve heat fluxes up to 1000 W/cm^2, as reported by Yang et al. [1]. Though several experiments (Pais et al. [2], Mudawar and Estes [3], Chow et al. [4], Mudawar [5], Lin and Ponnappan [6], Jiang and Dhir [7], and Rybicki and Mudawar [8]) had been conducted using spray cooling in recent years and various designs of spray-cooling devices are emerging, theoretical understanding of the spray-cooling heat-acquisition phenomena is still in its infancy. Even though spray cooling has been used in the industry for many years, the overall theoretical understanding is limited due to the complex interaction of spray-liquid-droplet impact on the evaporating thin liquid film over the hot surface, as illustrated in Fig. 1. Another complication to understanding the spray-cooling heat transfer mechanism is the small scales at which these phenomena occur. For example, the thin liquid film in which the nucleation takes place and heat is transferred had been measured to be anywhere from 1 to 350 μm (Pautsch et al. [9]). Measurement of

Received 4 October 2007; revision received 15 July 2008; accepted for publication 2 August 2008.

*James T. Womble Professor, Department of Civil Engineering, Computational Mechanics Laboratory, Bell 4190. Member AIAA.
†Graduate Research Assistant, Computational Mechanics Laboratory.
‡Senior Engineer, Power Division. Associate Fellow AIAA.
§Research Engineer. Senior Member AIAA.

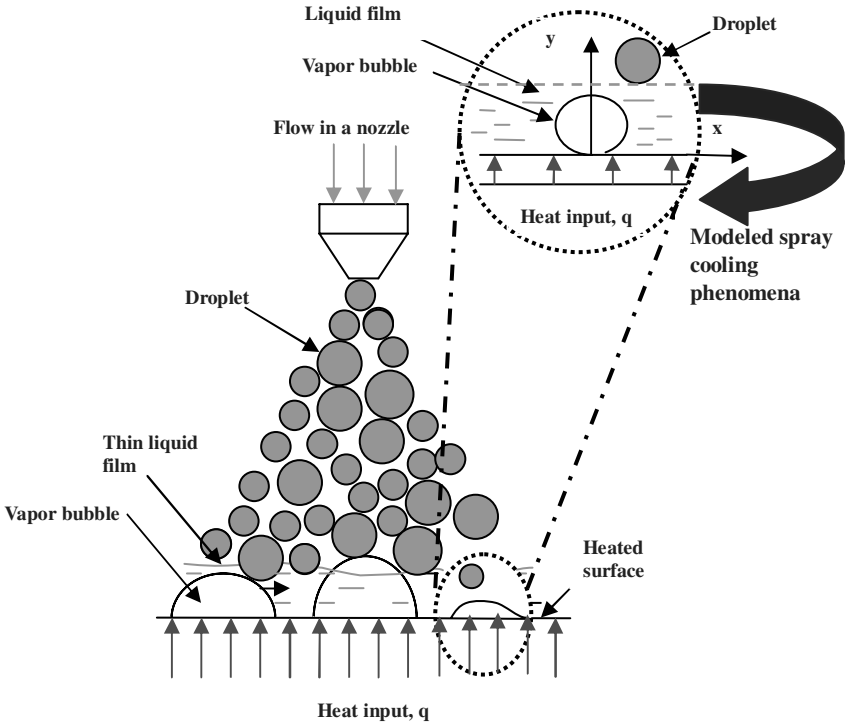

Fig. 1 Spray-cooling phenomena.

temperature and visualization of liquid–vapor-interface dynamics in such small thicknesses in which heat transfer and phase change occur during spray experimentation are very difficult. A focused effort to develop a comprehensive numerical model is of prime importance to this field.

Advances in computational power and efficiency led to abundant works in numerical simulation of multiphase flows, but very little work was available in numerical modeling of spray cooling, which will be discussed in some detail in a later subsection. The multiphase flow can be simulated using several methods such as the volume-of-fluid method introduced by Hirt and Nichols [10], level-set method introduced by Sussman et al. [11], and the marker-and-cell method. Limited modeling work is available in the related area of flow boiling [12–14], droplet impact on a hot plate, and some simplified models for spray cooling, but extensive research was performed in multiphase-flow modeling of different pool-boiling processes [15–24]. Recently, Son and Dhir [25] studied nucleate boiling heat transfer through multiphase-flow modeling. A detailed survey on the status of computer modeling of spray cooling and methods to solve multiphase flow was presented in Selvam et al. [26]. A survey on spray-cooling heat transfer was presented by Kim [27]. A brief review of modeling of spray cooling is discussed in the following subsection.

A. Spray-Cooling Modeling Review

Currently, there is no known published work that addresses modeling of the spray-cooling process as a whole that addresses several droplet formations, droplet impact onto the liquid film, vapor-bubble formation on the heated surface, and resulting heat transfers. A few empirical and numerical submodels are available that captured the heat transfer mechanism during the spray cooling, and a brief review of the modeling of spray cooling is presented here.

1. Empirical Model Review

Pautsch and Shedd [28] and Shedd and Pautsch [29] proposed a heat transfer equation based on their experimental results for single- and multiple-nozzle systems. They partitioned the heat transfer into a single-phase-dominated regime in and around the droplet impact region and a two-phase liquid film-boiling component in the corners away from this region. For multiple-nozzle spray, in addition to the two preceding regions, they considered a single-phase drainage-flow component between nozzles. They developed an empirical model based on these concepts; this model could predict the heat transfer for single- and multiple-nozzle arrays, and it was able to correlate their data with experimental results within 12%.

Chen et al. [30] attempted to model droplet and bubble dynamics and nucleate boiling heat transfer by tracking the lifetime of many bubbles nucleating within a liquid film. They assumed that bubbles nucleated from fixed sites randomly located or at multiple secondary nucleation sites around droplets impacting the liquid film. The predicted nucleate heat transfer was in agreement with experimental results. The authors concluded that fixed site nucleation was not an important factor. The results were sensitive to the secondary nuclei generated per droplet and bubble growth rate.

Sakamoto et al. [31] attempted to develop an empirical model that can predict 1×2 and 2×2 nozzle arrays. Using the measured heat flux for a single array, they predicted heat flux for multiple-nozzle systems. They proposed three different models, depending on different assumptions. In the best-fit model, single-nozzle heat transfer was used within a zone of influence, and in the interaction zone, they used superposition of the multiple-nozzle effect. Even though the model compared well overall with the measured value, when the local heat flux data were compared, there were discrepancies.

2. Analytical Model Review

Heat transfer mechanisms of spray cooling were analyzed, and an analytical model was developed using the volume-of-fluid numerical method by Yao et al. [32]. In this model, the average film thickness and the spray-cooling heat transfer behavior were predicted. Using the model, they studied the effect of droplet velocity and size on heat transfer and reported that the heat transfer was enhanced by increasing droplet velocity and reducing droplet size. However, they did not address the variation of thin film thickness with spray droplet size. Jia et al. [33] pointed out that Yao et al. [32] did not take into account the velocity slip and temperature jump. Jia et al. [33] developed a model based on continuity, momentum, and energy equations considering the velocity slip condition and temperature jump. The authors derived the heat transfer coefficient of the spray-cooling system. Some experiments were conducted to validate the established models.

3. Numerical Model Review

Modeling of spray cooling from fluid dynamics principles [including the process of liquid coming out from the nozzle, several droplet formation, droplet interaction, and droplet impact on liquid film with and without vapor bubble (as shown in Fig. 1)] is a highly challenging job at this time. In spray cooling, the heat is transferred from the hot plate by conduction, convection, and phase change of liquid. Selvam and Ponnappan [34] developed a two-dimensional model that captured the preceding heat transfer process in spray cooling using multiphase-flow modeling. This numerical spray-cooling model included one growing vapor bubble in thin liquid film and single-droplet impact (projected part on the top right side in Fig. 1) on the thin liquid film to understand the droplet and bubble dynamics and the high-heat-transfer mechanism in spray cooling. Even though the 2-D model cannot simulate three-dimensional effects of bubble and droplet dynamics, the model can explain certain important phenomena of heat transfer that are discussed subsequently. However, they computed a single-droplet impact over thin liquid film with single-vapor-bubble growth, and they could relate it to spray cooling because the symmetric boundary condition on each side made it the same as the effect of several droplets impacting on liquid film with several bubbles. In spray-cooling experiments, the liquid-film thickness varied from 1 to 350 μm and liquid-droplet diameter varied from 20 to 150 μm. In their model, liquid-film thickness and droplet diameter was around 44 and 40 μm, respectively. which represent the spray process. They described the multiphase-flow modeling by solving the incompressible Navier–Stokes equations using the level-set method to identify the liquid–vapor interface. The computer model used the finite difference method to discretize the governing equations.

Selvam et al. [35] studied the effect of the position of the vapor bubble and liquid droplet on heat removal in the computational domain and found the optimum position of the droplet with respect to the vapor bubble for effective heat removal for their model. The effect of droplet velocity and liquid-to-vapor density ratio was reported by Selvam et al. [36]. They found that the droplet velocity and density ratio both had an effect on heat transfer. Additionally, they reported that for higher density ratios, the trend of the Nusselt number Nu variation was the same as the lower density ratios, but the time step needed to be much smaller and resulted in more computational time. The effect of vapor-bubble size was considered by Selvam et al. [37]. It was observed that the maximum obtained heat flux increased with vapor-bubble size. The effect of convective flow on vapor-bubble dynamics and heat transfer was studied by Selvam et al. [38]. They observed that the maximum heat flux in terms of the Nusselt number increased with increased convective flow velocity, due to greater mass flow rate of cooler liquid over the heated surface and easy departure of the bubble from the hot surface. Selvam et al. [39] used the 2-D computer model to investigate the spray-cooling heat transfer phenomena. The heat transfer characteristics were investigated for two different cases. One was vapor-bubble growth and merging after bubble bursting. Another was liquid-droplet impact on thin liquid film with a growing vapor bubble. They identified and reported for the first time that transient conduction is the most important mechanism to achieve high heat flux in spray cooling.

They also studied the effects of micro- and macrogravity [40] using the 2-D computer model. They investigated the heat transfer from the hot wall during droplet impact and vapor-bubble growth for gravitational constants ranging 0.0001 to 2 g for small- and large-scale bubbles. It was found that the growth rate and heat transfer did not depend on the gravitational force for small bubbles, whereas they did for large bubbles. Finally, they concluded that for the droplet impingement, the heat transfer was not affected significantly by gravity.

The effect of thermal conductivity and latent heat of vaporization of liquid on heat transfer was studied by Selvam et al. [41]. They performed the conductivity study for different wall superheats and identified that for every wall superheat, the maximum heat flux linearly increased with conductivity. It was further identified that the effect of latent heat of vaporization on heat transfer in their model was not significant, but it affected the vaporization process. Recently, Selvam and Sarker [42] extended the multiphase-flow spray-cooling model in three dimensions and studied the effect of droplet velocity and wall superheat on heat transfer during spray cooling.

B. Scope of the Present Work

In spray cooling, each droplet acts as a small jet and cools the heated surface directly or mixes with the liquid over the heated plate. The spray liquid spreads on a wider area than with jet impingement. The heat is transferred due to conduction, convection, and phase change of liquid. The temperatures of the liquid thin film and the liquid droplet differ from the solid-heated-surface temperature. As a result, the temperature gradient develops within the liquid film, and the region of the fluid in which this temperature gradient exists is the thermal boundary layer. This thermal boundary layer evolves with time as the droplets impinge on the liquid layer continuously at different places. In the spray process, in which the cooler liquid droplet merges with hot liquid, the thickness of the thermal boundary layer is reduced locally due to cooling and in which the droplet does not merge for a while, the thickness increases as time goes on. This process happens continuously, and hence there is no steady thickness. The thermal-layer thickness in a particular area can also vary depending on spray droplet frequency. If the droplet frequency is lower, the temperature has a longer time to distribute within the thin liquid film and results in a thicker thermal layer during spray cooling. Similarly, the thermal-layer thickness is lower when droplet frequency is high. At present, there is no numerical model available that can predict the thermal-boundary-layer thickness in spray cooling. Furthermore, it is almost impossible to measure the thermal-boundary-layer thickness and study its effect on heat transfer and liquid–vapor dynamics by direct experimentation. Its effect may be very important. However, the thickness of thermal boundary can be varied and its effect can be illustrated using a numerical model. In the previous works [34–42], the initial thermal-layer thickness variation was not considered; only a very thin (8.8 μm) layer was assumed. In the present work, the effect of thermal layer on interface dynamics and the corresponding heat transfer are systematically investigated. This investigation helps to understand the influence of thermal-boundary-layer thickness on heat transfer in spray cooling. In addition, the mechanism of high heat flux is illustrated and will provide a better understanding of heat transfer phenomena in spray cooling.

II. Numerical Formulation for Multiphase Flow

Spray cooling is a very complex multiphase-flow process that includes several droplets formation from the nozzle, several bubble nucleations at the heated surface, droplet–bubble interactions, and resulting heat transfer (shown in Fig. 1). Currently, it is beyond the computational capabilities to model the whole process. However, a simplified part of the process (shown on the upper right side in Fig. 1), depending on the phenomena over the heated surface, is directly simulated.

The numerical formulation of multiphase flow is carried out by solving the incompressible Navier–Stokes equations. The level-set method is used to capture the liquid–vapor interface. For a survey on numerical techniques used to model multiphase flow, one can refer to Selvam et al. [26] and Tryggvason et al. [43]. For computer modeling of liquid and vapor, the level-set method introduced by Sussman et al. [11] for bubble dynamics, which was modified by Son and Dhir [44] to accommodate the effect of phase change, is used. The interface separating the two phases is captured by level-set function ϕ, which is defined as a positive or negative distance from the interface. Similar to Son and Dhir [44] and Son et al. [18], the negative sign is chosen for the vapor phase and the positive sign is chosen for the liquid phase. For more details on the level-set method and its application, one can refer to Sethian [45] and Osher and Fedkiw [46]. The extensive application of the level-set method in various areas of science and engineering were illustrated with their basic development in the preceding two books. Son [47] used the level-set method to model two incompressible fluid flows with an

immersed solid. The level-set method was modified to treat the contact-angle condition at the gas–liquid–solid interline and to incorporate a no-slip condition at the fluid–solid interface.

A. Governing Equations

In the present model, the fluid properties (including density, viscosity, specific heat, and thermal conductivity) are constant in each phase and the flow is assumed to be incompressible. The Navier–Stokes equations considering the effect of surface tension, gravity, and phase change at the interface are used and discussed as follows:

Momentum-conservation equation:

$$\rho(\partial_t \mathbf{u} + \mathbf{u}\cdot\nabla\mathbf{u}) = -\nabla p + \rho\mathbf{g} - \sigma\kappa\nabla H + \nabla\cdot\mu\nabla\mathbf{u} + \nabla\cdot\mu\nabla\mathbf{u}^T \tag{1}$$

Energy-conservation equation:

$$\rho c_p(\partial_t T + \mathbf{u}\cdot\nabla T) = \nabla\cdot k\nabla T - \rho(\mathbf{u}_{\text{int}} - \mathbf{u})h_{fg}\cdot\nabla H \tag{2}$$

The energy-balance condition at the interface is implemented implicitly in the preceding equation. The interfacial velocity $\mathbf{u}_{\text{int}}$ has to be obtained from the temperature condition at the interface, $T = T_{\text{sat}}$. To calculate the interfacial velocity, a Newtonian iteration algorithm was developed by Juric and Tryggvason [48]. This iteration algorithm requires expensive computations, and this is difficult to construct, as there is no explicit relation exists between the interfacial velocity and the interface temperature. To avoid such difficulty in solving the energy equation, the interfacial velocity $\mathbf{u}_{\text{int}}$ is extracted from the preceding equation, and the energy equation coupled with the interface-temperature condition is deduced as the following equation, as suggested by Son [49]:

$$\rho c_p(\partial_t T + \mathbf{u}\cdot\nabla T) = \nabla\cdot k\nabla T \quad \text{for } H > 0$$

$$T = T_{\text{sat}}(p_v) \quad \text{for } H = 0 \tag{3}$$

Mass-conservation equation:

$$\nabla\cdot\mathbf{u} = \mathbf{m}\cdot\nabla\rho/\rho^2 \tag{4}$$

To prevent instability at the interface the density, viscosity, and thermal conductivity are defined as

$$\rho = \rho_v + (\rho_l - \rho_v)H, \qquad \mu = \mu_v + (\mu_l - \mu_v)H$$
$$k = k_v + (k_l - k_v)H \tag{5}$$

where H is the Heaviside function and defined as

$$H = 1 \quad \text{if } \varphi \geq 1.5h, \qquad H = 0 \quad \text{if } \varphi \leq -1.5h$$
$$H = 0.5 + \frac{\varphi}{3h} + \sin\frac{2\pi\varphi/3h}{2\pi} \quad \text{if } |\varphi| \leq 1.5h \tag{6}$$

where h is a grid spacing and ϕ is a level-set function. Equation (6) implies that the interface separating two phases is replaced by a transition region of finite thickness. In this model, $3h$ spacing is used for the transition region.

The mass flux or volume source term included in the continuity equation (4) due to liquid–vapor phase change is derived from the conditions of mass continuity and energy balance at the interface:

Mass continuity at the interface:

$$\mathbf{m} = \rho(\mathbf{u}_{\text{int}} - \mathbf{u}) \tag{7}$$

Energy balance at the interface:

$$\mathbf{m} = k\nabla T/h_{fg} \tag{8}$$

Using the energy-balance relation at the interface, mass-conservation equation (4) becomes

$$\nabla\cdot\mathbf{u} = k\frac{\nabla T}{h_{fg}}\frac{\nabla\rho}{\rho^2} \tag{9}$$

Using the energy-balance relation at the interface, the equation of mass continuity at the interface [Eq. (7)] becomes

$$\mathbf{u}_{\text{int}} = \mathbf{u} + k\frac{\nabla T}{h_{fg}\rho_v} \tag{10}$$

In the level-set formulation, the level-set function ϕ is advanced by the interfacial velocity by solving the following equation:

$$\partial_t\varphi = -\mathbf{u}_{\text{int}}\cdot\nabla\varphi \tag{11}$$

Sussman et al. [11] discussed that this equation does not generally satisfy the condition that the level-set function should be maintained as a distance function to accurately calculate the interfacial curvature and steep density gradients. Hence, at each time step, the level-set function is reinitialized as follows (used by Son [49]):

$$\partial_t\varphi = \varphi_0(1 - |\nabla\varphi|)/\sqrt{(\varphi_0^2 + h^2)} \tag{12}$$

where ϕ_o is a solution of Eq. (11).

The surface-tension effect is considered in the momentum equation by using a step function H ($H = 0$ in the vapor and 1 in liquid) and κ is the interfacial curvature expressed for 2-D as

$$\kappa = \nabla\cdot(\nabla\varphi/|\nabla\varphi|) = \nabla\cdot n$$
$$= \left(\varphi_y^2\varphi_{xx} - 2\varphi_x\varphi_y\varphi_{xy} + \varphi_x^2\varphi_{yy}\right)/\left(\varphi_x^2 + \varphi_y^2\right)^{3/2} \tag{13}$$

The subscripts in the preceding equation represent differentiation. The surface-tension force $-\sigma\kappa\nabla H$ is implemented in the volume form to avoid the need for explicit description of the interface, as suggested by Brackbill et al. [50].

B. Nondimensional Form of the Governing Equations

The nondimensional form of the governing set of equations is derived using the characteristic length l_r, characteristic velocity u_r, characteristic time t_r, and dimensionless temperature T^*. They are defined as follows:

$$l_r = \sqrt{\frac{\sigma}{g_y(\rho_l - \rho_v)}}, \qquad u_r = \sqrt{g_y l_r}$$
$$t_r = \frac{l_r}{u_r} \quad \text{and} \quad T^* = \frac{T - T_{\text{sat}}}{T_w - T_{\text{sat}}} \tag{14}$$

where g_y represents the unit gravitational force in the y direction. The characteristic values are chosen in such a way that the gravity force becomes unity; that is, the Froude number Fr is equal to 1 and the Weber number We is just above 1.0 if the density ratio of liquid to vapor is large. In addition to the preceding scaling parameters, ρ, k, μ, and c_p of liquid are considered as reference values. The governing equations are nondimensionalized using the following nondimensional variables (denoted by asterisks):

$$x^* = \frac{x}{l_r}, \qquad y^* = \frac{y}{l_r}, \qquad t^* = \frac{t}{t_r}, \qquad \mathbf{u}^* = \frac{\mathbf{u}}{u_r}, \qquad \mathbf{g}^* = \frac{\mathbf{g}}{g_y}$$
$$T^* = \frac{T - T_{\text{sat}}}{T_{\text{wall}} - T_{\text{sat}}}, \qquad \rho^* = \frac{\rho}{\rho_l}, \qquad k^* = \frac{k}{k_l}, \qquad \mu^* = \frac{\mu}{\mu_l}$$
$$c_p^* = \frac{c_p}{c_{pl}}, \qquad p^* = \frac{p}{\rho_l u_r^2} \tag{15}$$

Using the preceding nondimensional variables, the governing nondimensional equations are as follows:

Nondimensional momentum equation:

$$\rho^*(\partial_{t^*}\mathbf{u}^* + \mathbf{u}^*\cdot\nabla\mathbf{u}^*) = -\nabla p^* + \frac{\rho^* g^*}{Fr^2} - \frac{\nabla\cdot n\nabla H}{We} + \frac{1}{Re}(\nabla\cdot\mu^*\nabla\mathbf{u}^* + \nabla\cdot\mu^*\nabla\mathbf{u}^{*T}) \tag{16}$$

Nondimensional energy equation:

$$\rho^* c_p^*(\partial_{t^*}T^* + \mathbf{u}^*\cdot\nabla T^*) = \frac{\nabla\cdot k^*\nabla T^*}{Pe} \tag{17}$$

Nondimensional mass-conservation equation:

$$\nabla\cdot\mathbf{u}^* = \frac{Jak^*\nabla T^*}{Pe}\cdot\frac{\nabla\rho^*}{\rho^{*2}} \tag{18}$$

Nondimensional mass-conservation equation at the interface:

$$\mathbf{u}^*_{\text{int}} = \mathbf{u}^* + \frac{Ja}{Pe}\frac{k^*\nabla T^*}{\rho^*} \tag{19}$$

where

$$Re = \frac{\rho_l u_r l_r}{\mu_l}, \qquad We = \frac{\rho_l u_r^2 l_r}{\sigma}, \qquad Ja = \frac{c_{pl}\Delta T}{h_{fg}}$$

$$Pe = \frac{\rho_l u_r l_r c_{pl}}{k_l}, \qquad Fr = \frac{u_r}{\sqrt{g l_r}}$$

III. Boundary Conditions

The boundary conditions for the governing equations are shown in Fig. 2 and are given as follows: At the wall ($y = 0$), $u = v = 0$, $T = T_w$, and $\phi_y = 0$. At the planes of symmetry ($x = 0$ and $x = x_{\max}$), $u = v_x = T_x = \phi_x = 0$. At the top of the computational domain (free surface, $y = y_{\max}$), $u_y = v_y = \phi_y = 0$ and $T = T_{\text{sat}}$.

IV. Numerical Solution

The governing equations (1), (3), (4), (11), and (12) combined together are highly nonlinear. The equations are discretized using the finite difference method on a staggered-grid system in which all the variables except pressure are stored at the grid points and pressure alone is stored at the cell center, as shown in Fig. 2. The diffusion terms are considered implicitly and the convection and source terms are considered explicitly in time. For spatial approximations, all terms are considered using second-order central difference and the convection term is considered using a second-order essentially nonoscillatory method, described by Chang et al. [51], to prevent numerical oscillations. The pressure and velocity are solved in a sequential manner by the procedure described by Selvam [52].

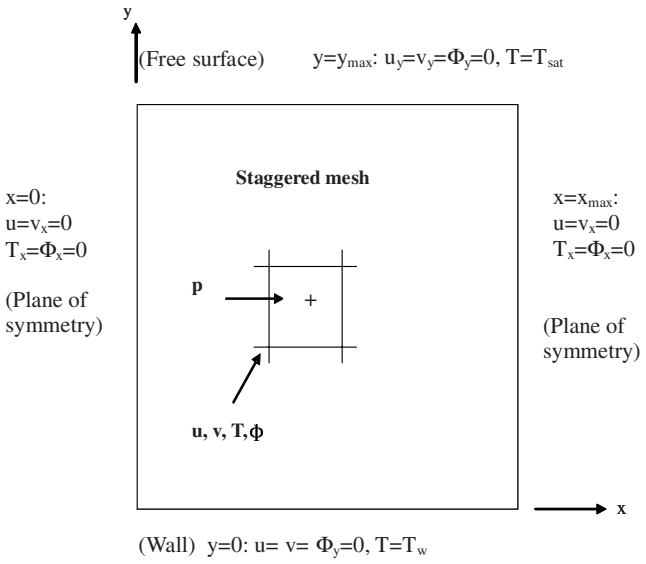

Fig. 2 Boundary condition and the location of variables stored in the staggered-grid system.

The discretized equations from the momentum, energy, and pressure equations are symmetric, and they are solved by the preconditioned conjugate gradient procedure (Ferziger and Peric [53]) in an iterative form. The iteration is done until the average residue for each node is reduced to less than 10^{-9}. This amount of accuracy is needed because of the high density difference between liquid and vapor. After assuming the initial position for distance functions at each time step, the equations are solved sequentially in the following order:

1) Solve momentum equation (1) for velocities.
2) Correct the velocity to take the pressure effect.
3) Solve the pressure Poison equation to satisfy continuity.
4) Update the velocities to include the new pressure effect.
5) Solve temperature equation (3).
6) Solve distance function equation (11).
7) Reinitialize the distance function as per Eq. (12) and go to the next time step.

During the computation, time steps were chosen to satisfy the Courant–Friedrichs–Lewy condition $\Delta t \le \min(h/(|u| + |v|), 10^{-6})$. This was done because of the explicit treatment of the convection terms and the condition that the numerical results should not change if the time steps are halved.

V. Simulation Details

A. Nondimensional Parameters

For this study, saturated FC-72 properties were taken. Here, the $T_{\text{sat}} = 53°\text{C}$ case is considered. For this temperature, the computed reference values are reference length $l_r = 736.2\ \mu\text{m}$, reference velocity $u_r = 85$ mm/s, and reference time $t_r = 8.66$ ms. The density ratio of liquid to vapor (ρ_l/ρ_v) is 138, and other nondimensional numbers are $Re = 218$, $We = 1.0$, $Pe = 2050$, and $Ja = 0.127$. In this study, the parameters considered are $\rho_l/\rho_v = 20$, $Re = 218$, $We = 1.0$, $Pe = 2050$, $Ja = 0.127$, and $\Delta T = 10°\text{C}$. A low density ratio is considered to reduce computer time and to avoid numerical instability. The computed results for a higher density ratio have a similar trend to a low density ratio, but the time step needs to be much smaller (Selvam and Ponnappan [34]).

B. Computational Domain and Initial Condition

The computational domain considered is 0.2×0.2 units, which is equal to $147 \times 147\ \mu\text{m}$. The computational domain is discretized by 201×201 meshes. The smallest grid is $0.74\ \mu\text{m}$. Time steps considered are 5×10^{-6} (43.3 ns) nondimensional time.

To study the effect of thermal-boundary-layer thickness on heat transfer and liquid–vapor-interface dynamics, a vapor bubble with a radius of 0.055 (40.49 μm) units in a liquid layer of 0.06 (44.17 μm) units is considered as the initial condition, as shown in Fig. 3a. A droplet radius of 0.03 (22 μm) units falling down with a speed of 30 (2.55 m/s) dimensionless units located at 0.13 (95.706 μm) units above the hot wall and 0.08 (58.896 μm) units from the left boundary is considered. In the spray-cooling experiment, the liquid-film thickness varies from 40 to 350 μm (Pautsch et al. [9]), liquid-droplet diameter varies between 20 to 190 μm (Chen et al. [54,55] and Baysinger et al. [56]), and spray velocity varies between 1 to 15 m/s (Baysinger et al. [56]). In this study, the liquid-layer thickness, the droplet diameter, and the droplet velocity are considered to be approximately 44 μm, 40 μm, and 2.55 m/s, respectively, which are in the range of experimental values. A vapor bubble with a diameter of 81 μm is considered.

In the actual spray-cooling experiment, the thermal-boundary-layer thickness in the thin liquid film is not known. In this modeling work, four different thermal-boundary-layer thicknesses [0.012 (9 μm), 0.022 (16.19 μm), 0.032 (23.56 μm), and 0.042 (30.92 μm)] are considered and their effect on

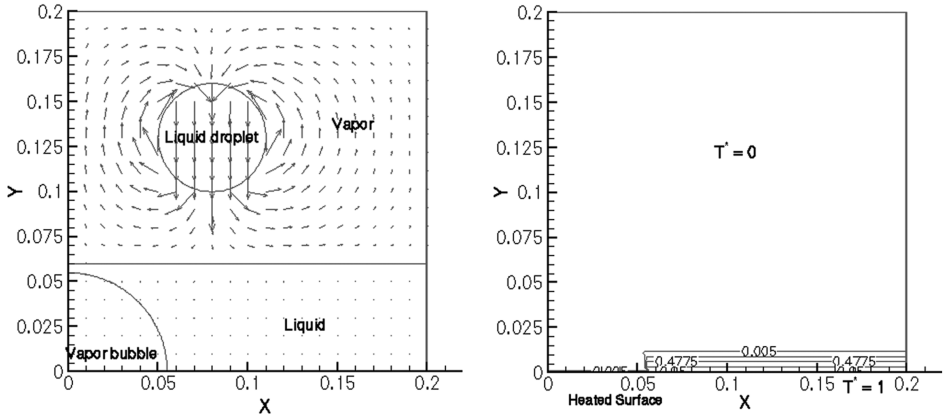

a) b)

Fig. 3 Initial a) velocity vector and liquid–vapor shape and b) temperature distribution.

liquid–vapor-interface dynamics (the mixing of hot and cooler liquids and corresponding heat transfer) is studied and reported.

The initial temperature distribution for 0.012 (9 μm) dimensionless units of thermal-layer thickness is shown in Fig. 3b, and for other thermal-layer thicknesses, the initial temperature distribution is similar, but the thickness is greater.

VI. Results and Discussion

A. Effect of Thermal-Boundary-Layer Thickness

The computed Nusselt number Nu and maximum velocity (in nondimensional units) of liquid and vapor (fluid) in the computational domain are shown in Fig. 4 for every thermal-boundary-layer thickness. From this figure, it is observed that for different thermal-layer thicknesses, the maximum average Nusselt number is different and is achieved at different time instants. The average Nusselt number takes a longer time to reach its first peak as the thermal-layer thickness increases. It is further observed that for a thicker thermal layer (0.022, 0.032, and 0.042 units), the Nusselt number distribution has two peaks and the second peak obtains the highest value.

Figures 5 and 6 show the liquid–vapor shape, velocity vector, temperature contour, and Nusselt number variation over the hot surface at different time instants for thermal-layer thicknesses of 0.012 (thinnest thermal layer) and 0.042 (thickest thermal layer) units, respectively. Though the Nusselt number variation with time is presented in Fig. 4, the Nusselt number variation along the hot wall is included at different time instants in Figs. 5 and 6 for better understanding of the high heat removal. The time, average Nusselt number, and maximum velocity at which the plots are made are reported in Tables 1 and 2, respectively, for thermal-layer thicknesses of 0.012 and 0.042 units.

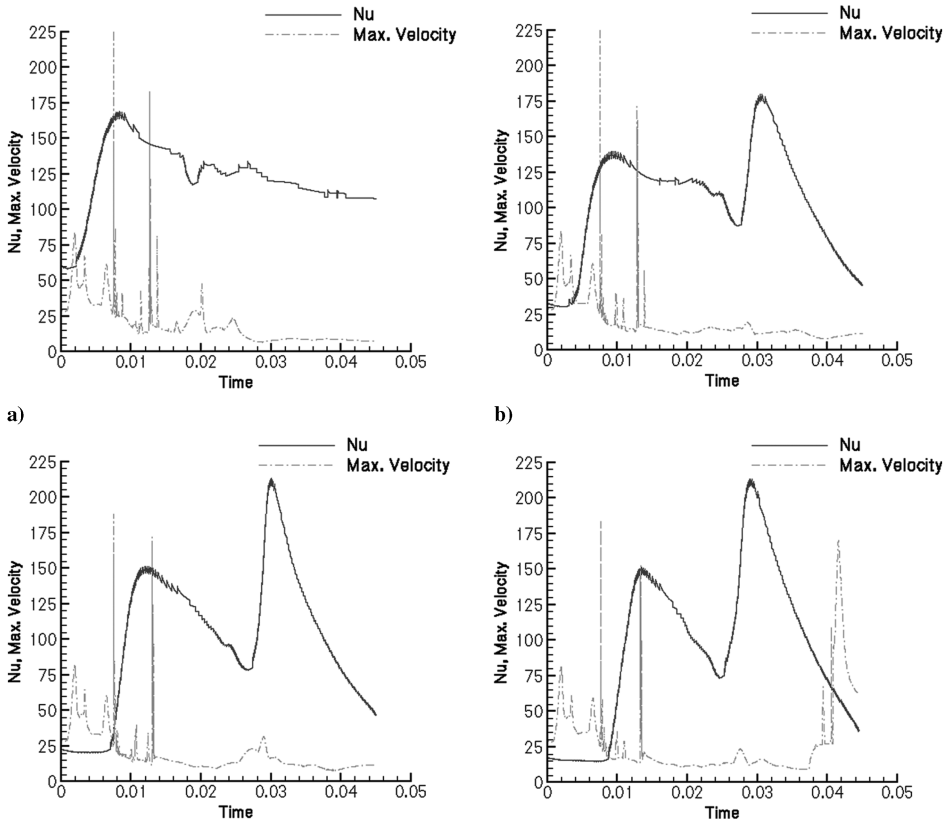

a) b) c) d)

Fig. 4 Nusselt number and maximum velocity variation: a) thermal boundary layer of 0.012 units, b) thermal boundary layer of 0.022 units, c) thermal boundary layer of 0.032, and d) thermal boundary layer of 0.042 units.

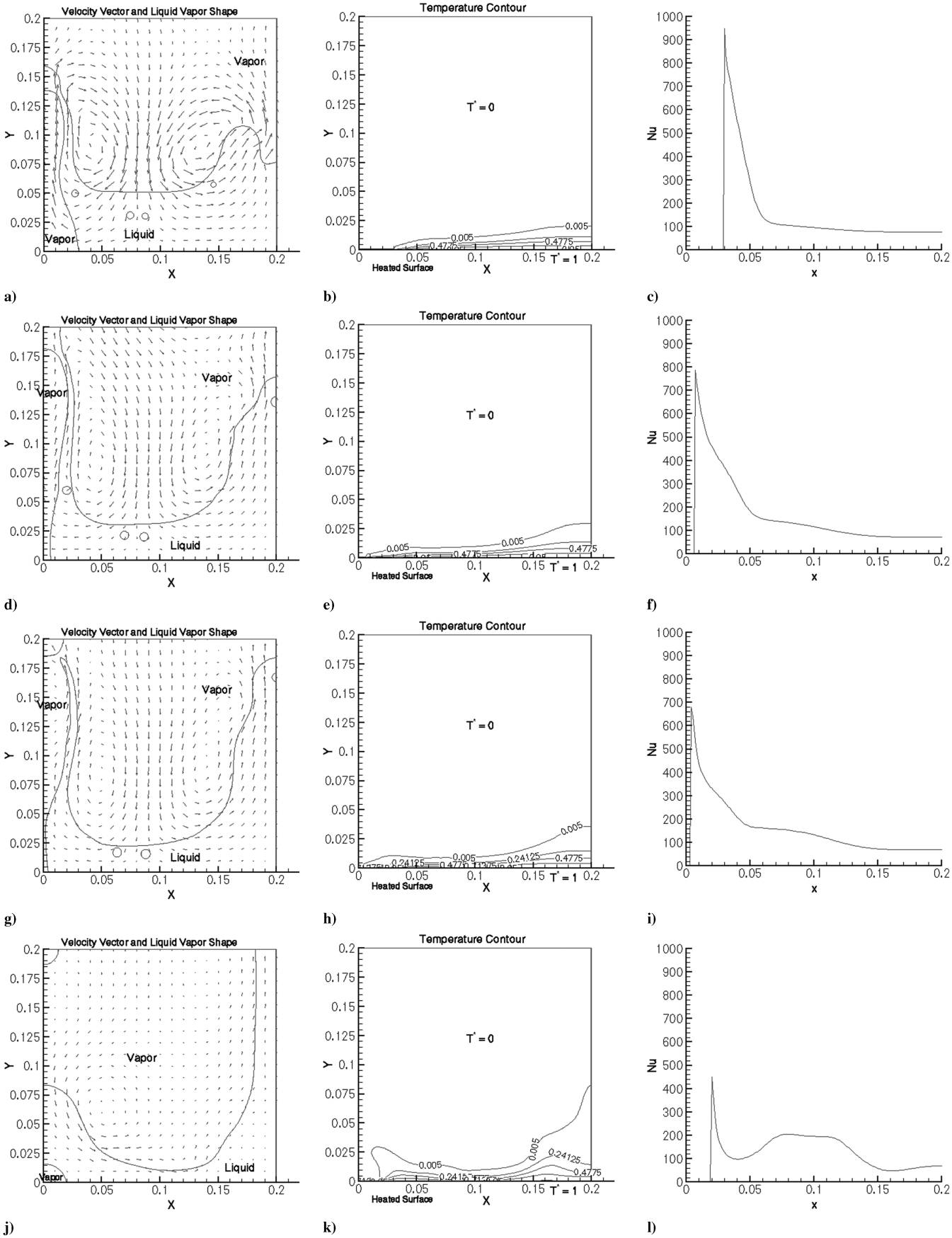

Fig. 5 Liquid vapor shape along with velocity vector (left), temperature distribution (middle), and Nusselt number variation (right) along the hot surface at a–c) 45.29 μs (during mixing of cold and hot liquid), d–f) 69.88 μs (near the Nusselt number peak value), g–i) 94.39 μs (near bubble bursting), and j–l) 266.73 μs for thermal-boundary-layer thickness of 0.012 units.

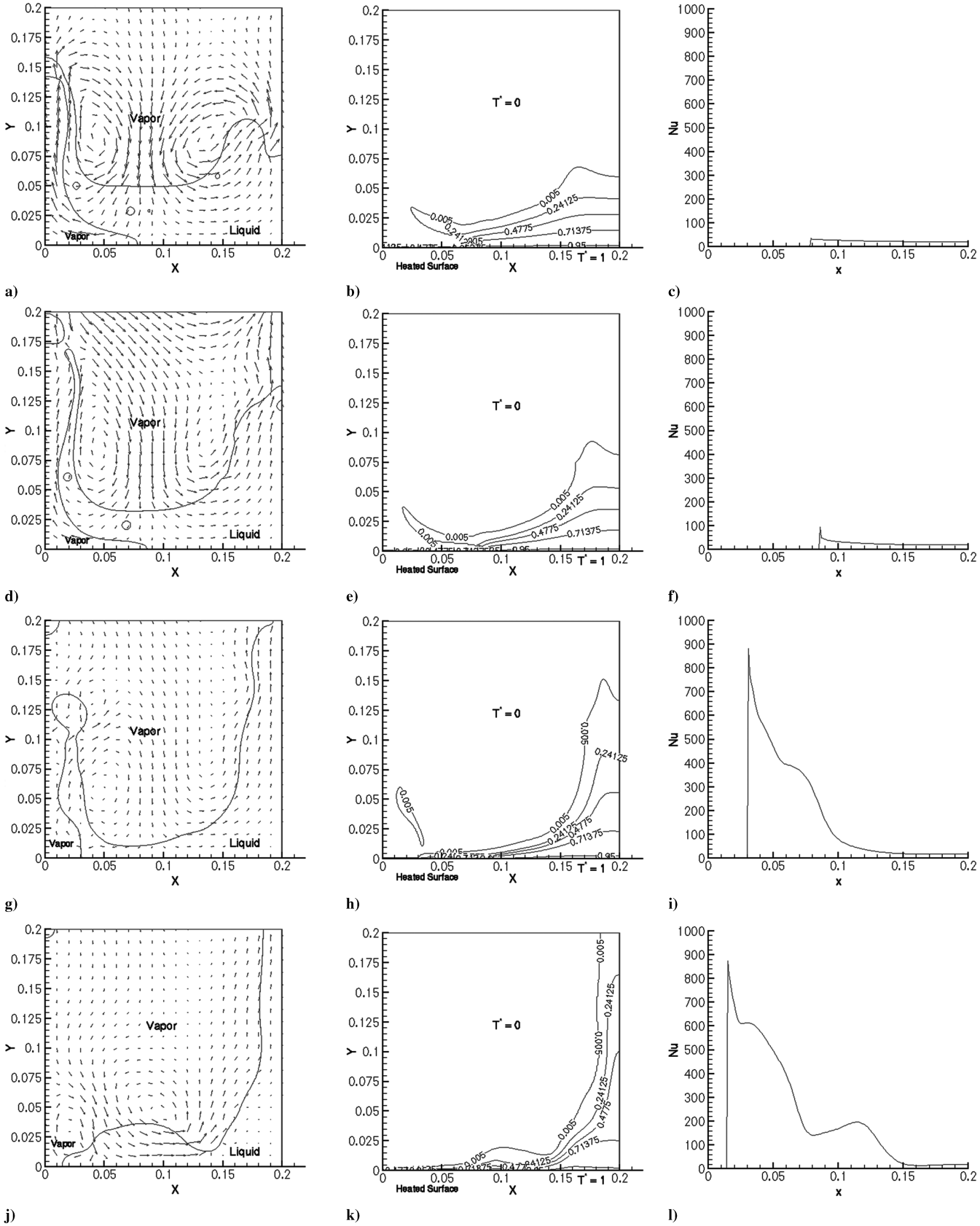

Fig. 6 Liquid vapor shape along with velocity vector (left), temperature distribution (middle), and Nusselt number variation (right) along the hot surface at a–c) 45.29 μs (during mixing of cold and hot liquid), d–f) 65.82 μs (near bubble bursting), g–i) 118.64 μs (near the first peak of the Nusselt number), and j–l) 250.27 μs (near the second peak of the Nusselt number) for thermal-boundary-layer thickness of 0.042 units.

Table 1 Average Nusselt number and maximum velocity for different time instants for thermal-layer thickness of 0.012 (8.8 μm)

Time	Average Nu	Maximum velocity
5.23×10^{-3} (45.29 μs)	132.14	33.49
8.07×10^{-3} (69.88 μs)	165.22	24.91
1.09×10^{-2} (94.39 μs)	154.99	16.19
3.08×10^{-2} (266.73 μs)	119.81	8.41

Table 2 Average Nusselt number and maximum velocity for different time instants for a thermal-layer thickness of 0.042 (30.92 μm)

Time	Average Nu	Maximum velocity
5.23×10^{-3} (45.29 μs)	15.13	35.33
7.60×10^{-3} (65.82 μs)	15.25	64.31
1.37×10^{-2} (118.64 μs)	148.86	20.49
2.89×10^{-2} (250.27 μs)	210.22	12.58

From Figs. 5a and 5b, it is observed that for a thinner thermal layer, the cold droplet mixes with more of the cold liquid (because the thermal layer is thin) and starts spreading over the dry area of the heated wall (Fig. 5d and 5e). But in a thicker thermal layer, a cold droplet impacted on the lesser amount of cold liquid (because the thermal layer is thick) mixes with more of the hot liquid and the temperature progresses above the vapor after the droplet impact (shown in Figs. 6a and 6b), which is not seen for thinner-thermal-layer cases. As a result, at that time, heat transfer is greater for a thinner thermal layer (comparing Figs. 5d and 5f and Figs. 6d and 6f).

Figures 5d–5f shows the liquid–vapor-interface dynamics, velocity vector, temperature contour, and variation of the Nusselt number over the hot surface near the peak value of the average Nusselt number (165.22) for a thermal-layer thickness of 0.012 units. Figures 6g–6i shows similar figures near the first peak of the average Nusselt number (148.86) for a thermal-layer thickness of 0.042 units. At this time, the average Nusselt number gets its maximum value for the thinnest thermal layer (0.012 units), whereas for thicker thermal layers (from 0.022 to 0.042 units), this first peak is not the maximum, the second peak is the maximum. The first peak of the Nusselt number is 148.86 and the second peak is 210.22 for thickest thermal boundary layer (0.042 units). When a droplet (i.e., the cold liquid) impacts and mixes with the liquid over the hot surface for each thermal layer, due to the impact, some amount of cold liquid starts moving upward and some moves toward the hot surface (as shown in Figs. 7–9). Because the density of the vapor is lower, the vapor bubble also tries to move upward. As a result, a portion of cold liquid moves and covers the dry region over the hot surface and, due to conduction and convection, more heat transfer occurs, which leads to the first peak of the Nusselt number.

For every run, the total amount of liquid over the hot surface is the same. As the thermal-boundary-layer thickness increases, the temperature progresses up to a greater height of liquid, and hence the amount of cold liquid near the hot surface decreases (as shown in Figs. 5d–5f and Figs. 6g–6i). Now for the thinnest thermal layer, the smaller thickness of thermal layer helps the heat transfer in two ways. First, there is less vaporization on the hot surface, and hence cold liquid can spread over a larger surface area of the hot plate (Figs. 5d and 5g); second, there is more cold liquid over the hot surface. Both of these factors help to remove more heat by conduction and convection, resulting in a higher Nusselt number value for the first peak. But for thicker thermal layers, there is more hot liquid over the hot surface, resulting in the formation of more vapor, and there is a smaller contact surface between the liquid and hot plate (Figs. 6d and 6g). The smaller amount of cold liquid also results in less heat transfer, and hence the Nusselt number is lower than the thinner-thermal-layer case for the first peak. The time taken for vapor-bubble bursting takes the least time for the thickest (0.042 units) thermal layer.

Figures 5j–5l show the shape of the liquid vapor along with velocity vector, temperature distribution, and Nusselt number variation along the hot surface for the thinnest thermal layer near the time instant at which the Nusselt number achieves the second peak for thicker-thermal-layer thicknesses (0.022 to 0.042 units). Figures 6j–6l shows similar plots near the time instant of the second peak of the average Nusselt number for a thermal-layer thickness of 0.042 units. Near this time, the average Nusselt number gets its maximum value for the thicker thermal layers (i.e., from 0.022 and 0.042 units), whereas for the thinnest thermal layer (i.e., for 0.012 units), this peak is absent. For the thinnest thermal layer, after the bubble bursting (when the cold liquid is coming back), it could not reach the hot surface (Fig. 5j–5l) because there was already liquid over the hot surface from the time instant of the first peak (i.e., no dry area), and the liquid is hot due to its long time contact with the hot surface (Figs. 5d–5i). Selvam et al. [39] identified the importance of moving the cooler liquid quickly to the heated dry surface, which causes the high heat flux due to transient conduction. Demiray and Kim [57] also concluded from their pool-boiling work that transient conduction/microconvection was the dominant mechanism for bubble heat transfer. Hence, for the thinnest thermal layer, the transient heat transfer could not take place at that time (Fig. 5l) and, as a result, no peak is observed. But for the thicker thermal layer (shown in Figs. 6j–6l), the high transient heat transfer could take place because the returning cold liquid spreads over the dry hot surface. As a result, the Nusselt number achieves the maximum value for the thicker thermal layer at this time. A very high and prolonged Nusselt number over the hot surface in Fig. 6l indicates the phenomena. From this study of the physical phenomena of the spray cooling, it may be said that transient conduction due to cold liquid spreading over the dry hot surface is the main reason for achieving high heat flux. The more contact area it gets over a dry hot surface for transient conduction, the greater the heat transfer.

B. Mechanism of High Heat Flux

From the previous discussion, it is clear that the transient conduction is the primary reason for high heat flux, but it has not been shown in detail how the transient conduction is happening. To explain the transient-conduction phenomena with detailed illustration, the heat transfer for the case of the thickest thermal boundary layer (0.042 units) is considered here.

1. Visualization of Interfaces and Discussion About the First Peak

Figures 7–13 show how the cold droplet impacts on the thin liquid film, impinges the liquid, replaces the vapor from the heated surface, and covers the dry area. Figure 7 shows the liquid–vapor dynamics and velocity-vector and temperature distribution just before the impact. Figures 8 and 9 show the similar plots after droplet impact, and from these figures, it is observed that some of the cold liquid moves upward and some of it impinges the liquid film (observed from the velocity-vector plot). Because the liquid near the hot wall is very hot, the liquid starts to vaporize, and the vapor is trying to cover the hot wall gradually (shown in Figs. 8–10). As the cold liquid droplet impinges the liquid film and the vapor starts to go upward due to impact and a lower density of vapor, the cold liquid replaces the vapor and covers the dry hot surface (shown in Figs. 11–13). In this way, the transient conduction is happening over that place and results in a higher Nusselt number (shown in Fig. 6i), which leads to the first peak of the Nusselt number.

2. Visualization of Interfaces and Discussion About the Second Peak

Figures 14–19 show how the cold liquid coming back again replaces the vapor from the heated surface and covers the dry area. Figures 14–17 show that the cold liquid is coming back from the left side of the domain. Figures 18 and 19 show that the rebounding cold liquid replaces the vapor over the hot surface for the second time. At this time, more cold liquid replaces the vapor and rewets the dry area and the high heat flux occurs (shown in Fig. 6l), which leads to the second peak of the Nusselt number.

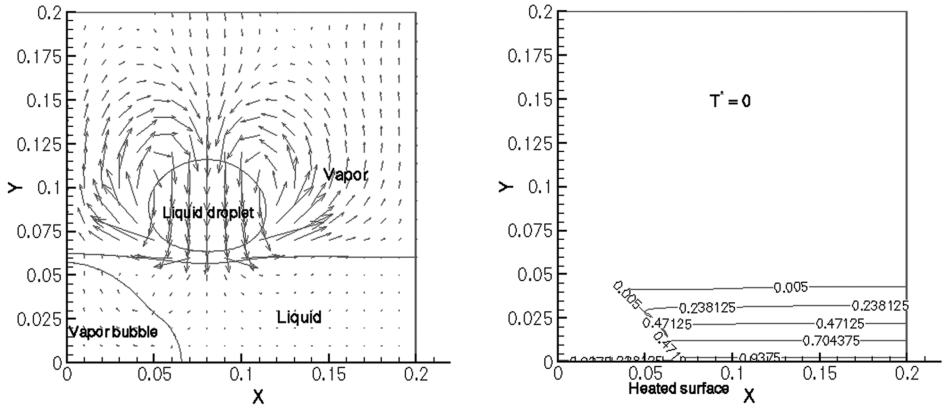

Fig. 7 Visualization of interface dynamics for the first peak of the Nusselt number for a thermal boundary layer of 0.042 at 13.47 μs.

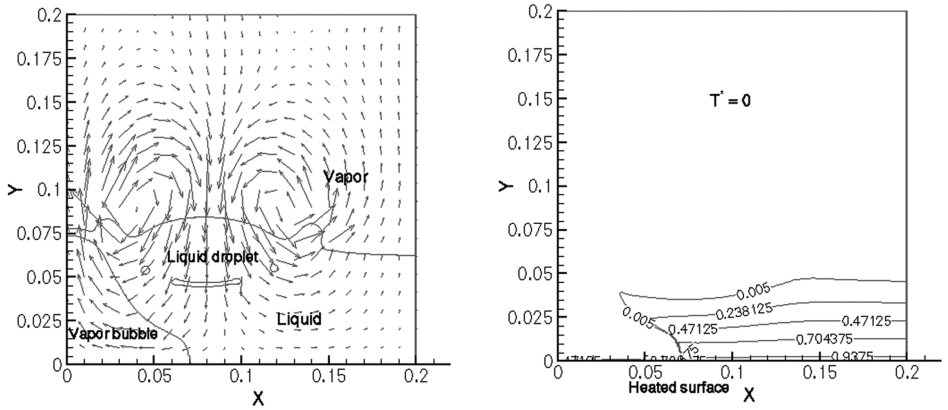

Fig. 8 Visualization of interface dynamics for the first peak of the Nusselt number for a thermal boundary layer of 0.042 at 24.20 μs.

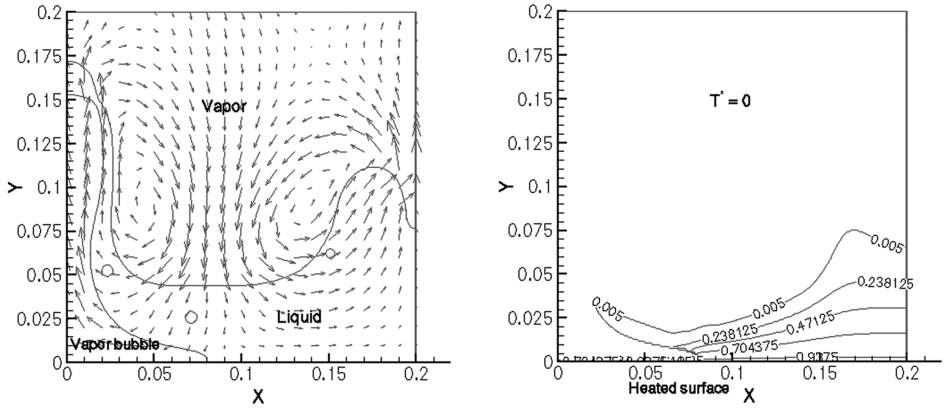

Fig. 9 Visualization of interface dynamics for the first peak of the Nusselt number for a thermal boundary layer of 0.042 at 51.05 μs.

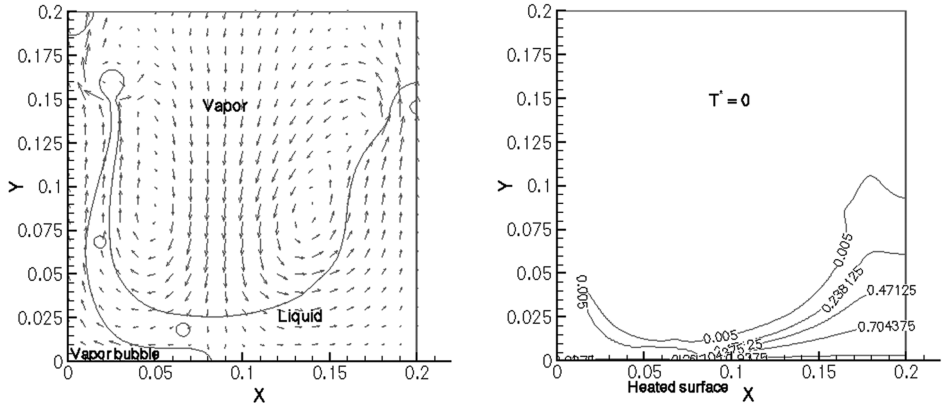

Fig. 10 Visualization of interface dynamics for the first peak of the Nusselt number for a thermal boundary layer of 0.042 at 77.89 μs.

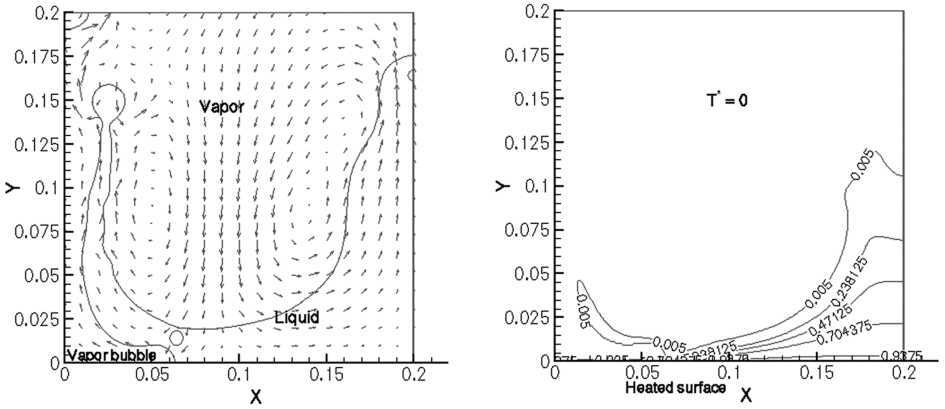

Fig. 11 Visualization of interface dynamics for the first peak of the Nusselt number for a thermal boundary layer of 0.042 at 91.23 μs.

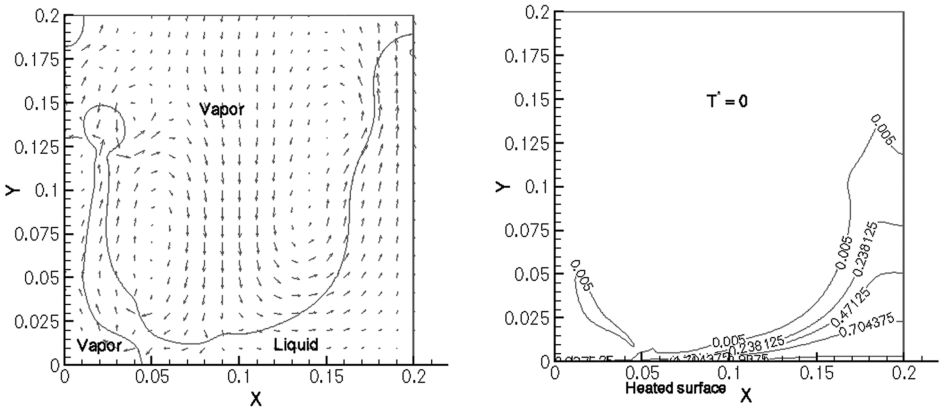

Fig. 12 Visualization of interface dynamics for the first peak of the Nusselt number for a thermal boundary layer of 0.042 at 104.66 μs.

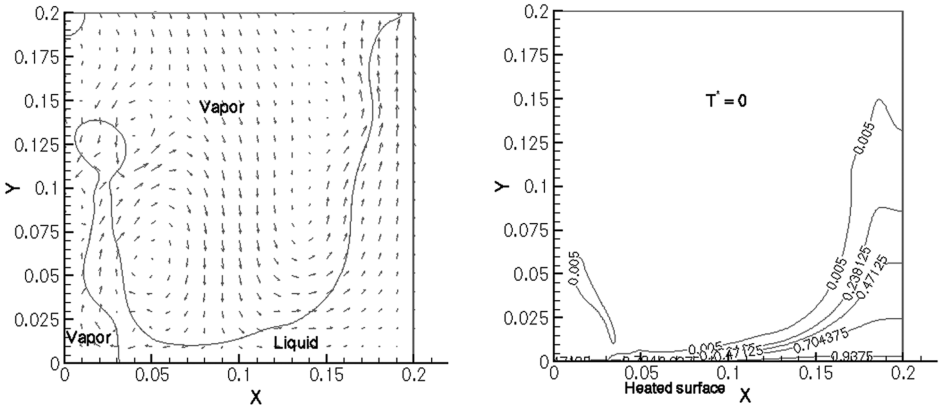

Fig. 13 Visualization of interface dynamics for the first peak of the Nusselt number for a thermal boundary layer of 0.042 at 117.95 μs.

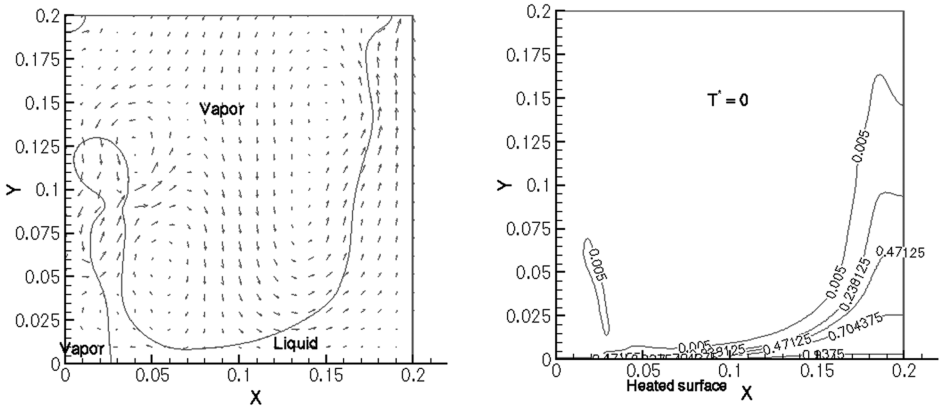

Fig. 14 Visualization of interface dynamics for the second peak value of the Nusselt number for a thermal boundary layer of 0.042 at 131.37 μs.

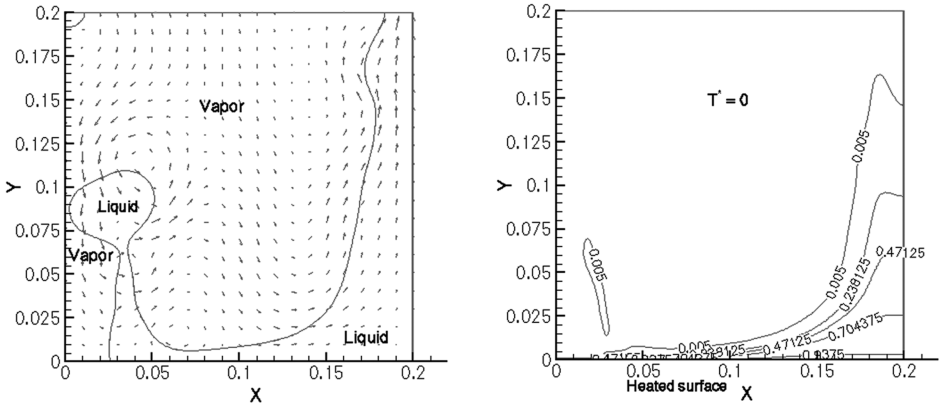

Fig. 15 Visualization of interface dynamics for the second peak value of the Nusselt number for a thermal boundary layer of 0.042 at 158.21 μs.

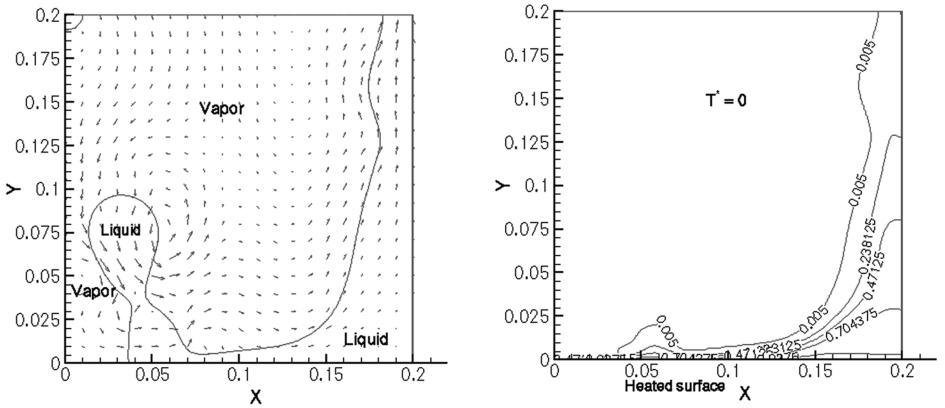

Fig. 16 Visualization of interface dynamics for the second peak value of the Nusselt number for a thermal boundary layer of 0.042 at 185.06 μs.

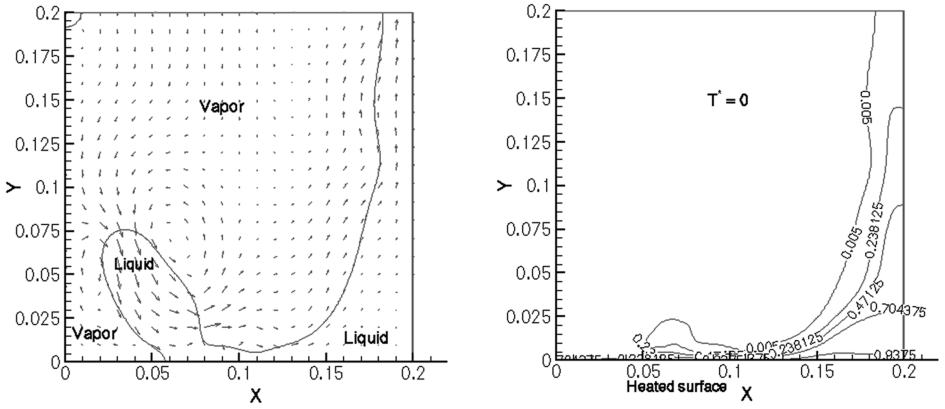

Fig. 17 Visualization of interface dynamics for the second peak value of the Nusselt number for a thermal boundary layer of 0.042 at 211.9 μs.

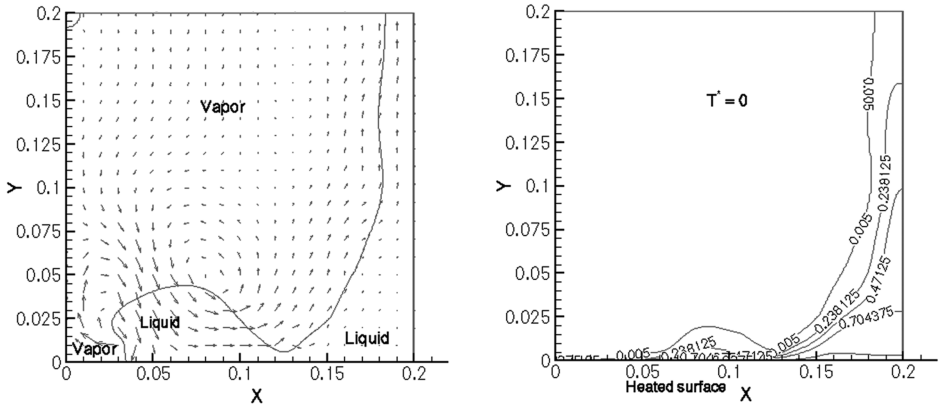

Fig. 18 Visualization of interface dynamics for the second peak value of the Nusselt number for a thermal boundary layer of 0.042 at 238.76 μs.

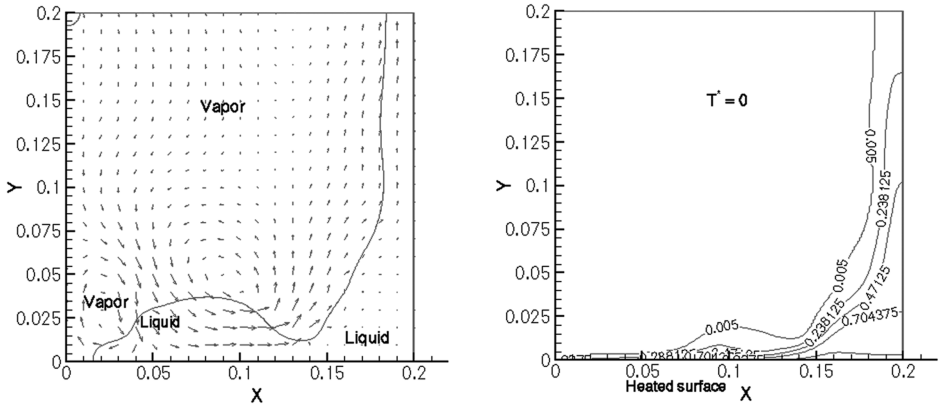

Fig. 19 Visualization of interface dynamics for the second peak value of the Nusselt number for a thermal boundary layer of 0.042 at 249.49 μs.

VII. Conclusions

The effect of thermal-boundary-layer thickness on liquid–vapor-interface dynamics and the high-heat-transfer mechanism was investigated in this study. Numerical modeling of two-phase flow is done using the level-set method. For each thermal-layer thickness, this computer model is used to study the interface dynamics and high-heat-transfer phenomena in the microenvironment of about 44-μm-thick liquid layer with droplet impact and vapor-bubble growing and bursting. From the study, the following conclusions are made:

1) The cold-droplet impingement during impact, rebound of cold liquid after impact, and transient conduction due to spreading of cold liquid over the dry hot surface are found to be the dominant mechanisms for higher heat flux. This mechanism is different from the widely accepted view that microlayer evaporation is the dominant heat transfer mechanism in saturated pool boiling.

2) The temperature distribution and liquid–vapor-interface movement in the computational domain is different for different thermal-layer thicknesses.

3) For different thermal-layer thicknesses, the maximum average Nusselt number is different and is achieved at different time instants. It is further observed that the Nusselt number distribution over time has two peaks for thicker thermal layers (i.e., for 0.022, 0.032 and 0.042 units) and the second peak is the maximum, whereas for the thinnest thermal layer, it has one peak.

4) As the thermal-boundary-layer thickness increases, the temperature progresses up to a greater height of liquid, and hence the amount of cold liquid over the hot surface decreases. For the thinnest thermal layer, the smaller thickness of the thermal layer helps the heat transfer in two ways. First, there is less vaporization on the hot surface, and hence cold liquid can spread over a larger surface area of the hot plate; second, there is more cold liquid over the hot surface. Both of these help to remove more heat by conduction and convection, resulting in a higher Nusselt number value for the first peak. For a thicker thermal layer, the hot liquid is over more of the hot surface, resulting in the formation of more vapor, and there is a smaller contact surface between the liquid and hot plate. The lower amount of cold liquid also results in less heat transfer by conduction and convection, and hence the Nusselt number is lower than the thinner-thermal-layer case for the first peak.

5) For a thicker thermal layer, most of the upward-moving cold liquid starts to come back toward the hot surface, and a larger amount of cold liquid mixes with the liquid placed there and results in more spreading over the hot plate. More contact area and more cold liquid over the hot surface helps with more conduction and convection and hence more heat transfer during the second peak for the thicker thermal layer.

Acknowledgments

The first three authors acknowledge the support received from the Propulsion Directorate's Power Division, U.S. Air Force Research Laboratory, through the Universal Technology Corporation research grant F33615-02-D-2299 and the Office of Naval Research "Defense Experimental Program to Stimulate Competitive Research" grant through the University of Arkansas to perform this work and the encouragement provided by J. Balda, Department of Electrical Engineering, University of Arkansas.

References

[1] Yang, J. L., Chow, C., and Paris, M. R., "Nucleate Boiling Heat Transfer in Spray Cooling," *Journal of Heat Transfer*, Vol. 118, No. 3, 1996, pp. 668–671. doi:10.1115/1.2822684

[2] Pais, M. R., Chow, L. C., and Mahefkey, E. T., "Surface Roughness and Its Effects on the Heat Transfer Mechanism in Spray Cooling," *Journal of Heat Transfer*, Vol. 114, No. 1, 1992, pp. 211–219. doi:10.1115/1.2911248

[3] Mudawar, I., and Estes, K. A., "Optimizing and Predicting CHF in Spray Cooling of a Square Surface," *Journal of Heat Transfer*, Vol. 118, No. 3, 1996, pp. 672–679. doi:10.1115/1.2822685

[4] Chow, L. C., Sehembey, M. S., and Pais, M. R., "High Heat Flux Spray Cooling," *Annual Review of Heat Transfer*, Vol. 8, 1997, pp. 291–318.

[5] Mudawar, I., "Assessment of High Heat-Flux Thermal Management Schemes," *IEEE Transactions on Components and Packaging Technologies*, Vol. 24, No. 2, 2001, pp. 122–141. doi:10.1109/6144.926375

[6] Lin, L., and Ponnappan, R., "Heat Transfer Characteristics of Spray Cooling in a Close Loop," *International Journal of Heat and Mass Transfer*, Vol. 46, No. 20, 2003, pp. 3737–3746. doi:10.1016/S0017-9310(03)00217-5

[7] Jiang, S., and Dhir, V. K., "Spray Cooling in a Closed System with Different Fractions of Non-Condensibles in the Environment," *International Journal of Heat and Mass Transfer*, Vol. 47, No. 25, 2004, pp. 5391–5406. doi:10.1016/j.ijheatmasstransfer.2004.07.013

[8] Rybicki, J. R., and Mudawar, I., "Single-Phase and Two-Phase Cooling Characteristics of Upward-Facing Sprays," *International Journal of Heat and Mass Transfer*, Vol. 49, Nos. 1–2, 2006, pp. 5–16. doi:10.1016/j.ijheatmasstransfer.2005.07.040

[9] Pautsch, A. G., Shedd, T. A., and Nellis, G. F., "Thickness Measurements of the Thin Film in Spray Evaporative Cooling," *Ninth Intersociety Conference on Thermal and Thermomechanical Phenomena in Electronic Systems*, Inst. of Electrical and Electronics Engineers, Piscataway, NJ, 2004, pp. 70–76.

[10] Hirt, C. W., and Nichols, B. D., "Volume of Fluid (VOF) Method for the Dynamics of Free Boundaries," *Journal of Computational Physics*, Vol. 39, No. 1, 1981, pp. 201–225. doi:10.1016/0021-9991(81)90145-5

[11] Sussman, M., Smereka, P., and Osher, S., "A Level Set Approach for Computing Solutions to Incompressible Two-Phase Flow," *Journal of Computational Physics*, Vol. 114, No. 1, 1994, pp. 146–159. doi:10.1006/jcph.1994.1155

[12] Mukherjee, A., and Kandlikar, S. G., "Numerical Simulation of Growth of a Vapor Bubble During Flow Boiling of Water in a Microchannel," *Microfluidics and Nanofluidics*, Vol. 1, No. 2, May 2005, pp. 137–145. doi:10.1007/s10404-004-0021-8

[13] Mukherjee, A., and Kandlikar, S. G., "Numerical Study of the Effect of Surface Tension on Vapor Bubble Growth During Flow Boiling in Microchannels," Fourth International Conference on Nanochannels, Microchannels and Minichannels, American Society of Mechanical Engineers Paper ICNMM2006-96050, Limerick, Ireland, 2006.

[14] Mukherjee, A., "Numerical Study of Conjugate Heat Transfer Due to Growth of a Vapor Bubble During Flow Boiling of Water in a Microchannel," 2007 ASME-JSME Thermal Engineering Summer Heat Transfer Conference, American Society of Mechanical Engineers Paper HT2007-32434, Vancouver, British Columbia, Canada, 2007.

[15] Welch, S. W. J., "Direct Simulation of Vapor Bubble Growth in Nucleate Boiling from Inception Through Departure," *International Journal of Heat and Mass Transfer*, Vol. 41, No. 12, 1998, pp. 1655–1666.
doi:10.1016/S0017-9310(97)00285-8

[16] Son, G., Dhir, V. K., and Ramanujapu, N., "Dynamics and Heat Transfer Associated with a Single Bubble During Nucleate Boiling on a Horizontal Surface," *Journal of Heat Transfer*, Vol. 121, No. 3, 1999, pp. 623–631.
doi:10.1115/1.2826025

[17] Dhir, V., "Numerical Simulation of Pool Boiling Heat Transfer," *AIChE Journal*, Vol. 47, No. 4, 2001, pp. 813–834.
doi:10.1002/aic.690470407

[18] Son, G., Ramanujapu, N., and Dhir, V., "Numerical Simulation of Bubble Merger Process on a Single Nucleation Site During Pool Nucleate Boiling," *Journal of Heat Transfer*, Vol. 124, No. 1, 2002, pp. 51–62.
doi:10.1115/1.1420713

[19] Abarajith, H. S., and Dhir, V. K., "A Numerical Study of the Effect of Contact Angle on the Dynamics of a Single Bubble During Pool Boiling," *International Mechanical Engineering Conference and Exposition*, American Society of Mechanical Engineers Paper 2002-33876, New Orleans, LA, 2002.

[20] Abarajith, H. S., Dhir, V. K., Warrier, G., and Son, G., "Numerical Simulation and Experimental Validation of the Dynamics of Multiple Bubble Merger During Pool Boiling Under Microgravity Condition," *Annals of the New York Academy of Sciences*, Vol. 1027, Nov. 2004, pp. 235–258.
doi:10.1196/annals.1324.020

[21] Esmaeeli, A., and Tryggvason, G., "Computations of Film Boiling Part 1: Numerical Method," *International Journal of Heat and Mass Transfer*, Vol. 47, No. 25, 2004, pp. 5451–5461.
doi:10.1016/j.ijheatmasstransfer.2004.07.027

[22] Esmaeeli, A., and Tryggvason, G., "Computations of Film Boiling Part 2: Multimode Film Boiling," *International Journal of Heat and Mass Transfer*, Vol. 47, No. 25, 2004, pp. 5463–5476.
doi:10.1016/j.ijheatmasstransfer.2004.07.028

[23] Mukherjee, A., and Dhir, V. K., "Study of Lateral Merger of Vapor Bubbles during Nucleate Pool Boiling," *Journal of Heat Transfer*, Vol. 126, No. 6, 2004, pp. 1023–1039.
doi:10.1115/1.1834614

[24] Shin, S., Abdel-Khalik, S. I., and Juric, D., "Direct Three-Dimensional Numerical Simulation of Nucleate Boiling Using the Level Contour Reconstruction Method," *International Journal of Multiphase Flow*, Vol. 31, Nos. 10–11, 2005, pp. 1231–1242.

[25] Son, G., and Dhir, V. K., "Numerical Simulation of Nucleate Boiling on a Horizontal Surface at High Heat Fluxes," *International Journal of Heat and Mass Transfer*, Vol. 51, Nos. 9–10, 2008, pp. 2566–2582.
doi:10.1016/j.ijheatmasstransfer.2007.07.046

[26] Selvam, R. P., Lin, L., and Ponnappan, R., "Computational Modeling of Spray Cooling: Current Status and Future Challenges," *Space Technology and Applications International Forum*, American Inst. of Physics, Melville, NY, 2005, pp. 56–63.

[27] Kim, J., "Spray Cooling Heat Transfer: The State of the Art," *International Journal of Heat and Fluid Flow*, Vol. 28, No. 4, 2007, pp. 753–767.
doi:10.1016/j.ijheatfluidflow.2006.09.003

[28] Pautsch, A. G., and Shedd, T. A., "Spray Impingement Cooling with Single- and Multiple-Nozzle Arrays Part 1: Heat Transfer Data Using FC-72," *International Journal of Heat and Mass Transfer*, Vol. 48, No. 15, 2005, pp. 3167–3175.
doi:10.1016/j.ijheatmasstransfer.2005.02.012

[29] Shedd, T. A., and Pautsch, A. G., "Spray Impingement Cooling with Single- and Multiple-Nozzle Arrays Part 2: Visualization and Empirical Models," *International Journal of Heat and Mass Transfer*, Vol. 48, No. 15, 2005, pp. 3176–3184.
doi:10.1016/j.ijheatmasstransfer.2005.02.013

[30] Chen, R. H., Tan, D. S., Lin, Juo-Chi., Chow, L. C., Griffin, A. R., and Rini, D. P., "Droplet and Bubble Dynamics in Saturated FC-72 Spray Cooling," International Mechanical Engineering Conference and Exposition, Orlando, FL, American Society of Mechanical Engineers Paper IMECE2005-80456, 2005.

[31] Sakamoto, H., Kim, J., Kiger, K., and Steinthorrson, E., "Multi-Nozzle Spray Cooling: Effects of Spray Interaction," *Annals of the Assembly for International Heat Transfer Conference 13*, Begell House, Redding, CT, 2006.
doi:10.1615/IHTC13.p12.370

[32] Yao, W., Analysis and Design of a Spray Cooling Thermal Control System for Spacecraft High Power Density Components," 57th International Astronautical Congress, International Astronautical Federation Paper IAC-06-C2.P.2.03, Oct. 2006.

[33] Jia, J., Guo, Y., and Wang, W., "Modeling and Experimental Research on Spray Cooling," *24th Annual IEEE Semiconductor Thermal Measurement and Management Symposium (Semi-Therm 2008)*, Inst. of Electrical and Electronics Engineers, Piscataway, NJ,2008, pp. 118–123.

[34] Selvam, R. P., and Ponnappan, R., "Numerical Modeling of Nucleation Boiling in Thin Film and Effect of Droplet Impact," *Thermal and Fluids Analysis Workshop (TFAWS 2004)*, NASA Ames Research Center, Moffett Field, CA, 2004.

[35] Selvam, R. P., Baskara, S., Balda, J. C., Barlow, F., and Elshabini, A., "Computer Modeling of Liquid Droplet Impact on Heat Transfer During Spray Cooling," American Society of Mechanical Engineers Paper HT2005-72569, 2005.

[36] Selvam, R. P., Sarkar, M., and Ponnappan, R., "Modeling of Spray Cooling: Effect of Droplet Velocity and Liquid to Vapor Density Ratio on Heat Transfer," *Thermal and Fluids Analysis Workshop (TFAWS 2005)*, NASA Ames Research Center, Moffett Field, CA, 2005.

[37] Selvam, R. P., Sarkar, M., Sarkar, S., and Ponnappan, R., "Effect of Vapor Bubble Size on Heat Transfer in Spray Cooling," *Space Technology and Applications International Forum*, Vol. 813, American Inst. of Physics, Melville, NY, 2006, pp. 145–152.

[38] Selvam, R. P., Sarkar, S., and Ponnappan, R., "Modeling of Spray Cooling: Convective Flow Effect on Vapor Bubble Dynamics and Heat Transfer," 9th AIAA/ASME Joint Thermophysics and Heat Transfer Conference, AIAA Paper 2006-3411, San Francisco, 2006.

[39] Selvam, R. P., Lin, L., and Ponnappan, R., "Direct Simulation of Spray Cooling: Effect of Vapor Bubble Growth and Liquid Droplet Impact on Heat Transfer," *International Journal of Heat and Mass Transfer*, Vol. 49, Nos. 23–24, 2006, pp. 4265–4278.
doi:10.1016/j.ijheatmasstransfer.2006.05.009

[40] Selvam, R. P., Hamilton, M., and Silk, E. A., "Modeling of Spray Cooling: Droplet Impact and Vapor Bubble Growth Effects on Heat Transfer in Micro and Macro-Gravity," *Thermal and Fluids Analysis Workshop (TFAWS 2006)*, NASA Ames Research Center, Moffett Field, CA, 2006.

[41] Selvam, R. P., Sarkar, M., and Ponnappan, R., "Effect of Thermal Conductivity and Latent Heat of Vaporization of Liquid on Heat Transfer in Spray Cooling," Society of Automotive Engineers Paper 2006-01-3068, 2006.

[42] Selvam, R. P., and Sarkar, S., "Understanding High Heat Transfer in Spray Cooling for Different Droplet Velocities and Wall Superheat by 3-D Multiphase Flow Modeling," *Proceedings of ASME-JSME Thermal Engineering Summer Heat Transfer Conference*, American Society of Mechanical Engineers, Paper HT2007-323132007.

[43] Tryggvason, G., Bunner, B., Esmaeeli, A., Juric, D., Al-Rawahi, N., Tauber, W., Han, J., Nas, S., and Jan, Y. J., "A Front-Tracking Method for the Computations of Multiphase Flow," *Journal of Computational Physics*, Vol. 169, No. 2, 2001, pp. 708–759.
doi:10.1006/jcph.2001.6726

[44] Son, G., and Dhir, V. K., "Numerical Simulation of Film Boiling Near Critical Pressures with a Level Set Method," *Journal of Heat Transfer*, Vol. 120, No. 1, 1998, pp. 183–192.
doi:10.1115/1.2830042

[45] Sethian, J. A., "Level Set Methods and Fast Marching Methods: Evolving Interfaces in Computational Geometry," *Fluid Mechanics*, Computer Vision and Material Science, Cambridge Univ. Press, Cambridge, England, U.K., 1999.

[46] Osher, S., and Fedkiw, R., *Level Set Methods and Dynamic Implicit Surfaces*, Springer, New York, 2003.

[47] Son, G., "A Level Set Method for Incompressible Two-Fluid Flows with Immersed Solid Boundaries," *Numerical Heat Transfer, Part B, Fundamentals*, Vol. 47, No. 5, 2005, pp. 473–489.
doi:10.1080/10407790590919252

[48] Juric, D., and Tryggvason, G., "Computations of Boiling Flows," *International Journal of Multiphase Flow*, Vol. 24, No. 3, 1998, pp. 387–410.
doi:10.1016/S0301-9322(97)00050-5

[49] Son, G., "A Numerical Method for Bubble Motion with Phase Change," *Numerical Heat Transfer, Part B, Fundamentals*, Vol. 39, No. 5, 2001, pp. 509–523. doi:10.1080/104077901750188868

[50] Brackbill, J. U., Kothe, D. B., and Zamach, C., "A Continuum Method for Modeling Surface Tension," *Journal of Computational Physics*, Vol. 100, No. 2, 1992, pp. 335–354. doi:10.1016/0021-9991(92)90240-Y

[51] Chang, Y. C., Hou, T. Y., Merriman, B., and Osher, S., "A Level Set Formulation of Eulerian Interface Capturing Methods for Incompressible Fluid Flows," *Journal of Computational Physics*, Vol. 124, No. 2, 1996, pp. 449–464. doi:10.1006/jcph.1996.0072

[52] Selvam, R. P., "Computation of Pressures on Texas Tech Building Using Large Eddy Simulation," *Journal of Wind Engineering and Industrial Aerodynamics*, Vols. 67–68, Apr.–June 1997, pp. 647–657. doi:10.1016/S0167-6105(97)00107-4

[53] Ferziger, J. H., and Peric, M., *Computational Methods for Fluid Dynamics*, Springer, New York, 2002.

[54] Chen, R. H., Chow, L. C., and Navedo, J. E., "Effects of Spray Characteristics on Critical Heat Flux in Subcooled Water Spray Cooling," *International Journal of Heat and Mass Transfer*, Vol. 45, No. 19, 2002, pp. 4033–4043. doi:10.1016/S0017-9310(02)00113-8

[55] Chen, R. H., Chow, L. C., and Navedo, J. E., "Optimal Spray Characteristic in Water Spray Cooling," *International Journal of Heat and Mass Transfer*, Vol. 47, No. 23, 2004, pp. 5095–5099. doi:10.1016/j.ijheatmasstransfer.2004.05.033

[56] Baysinger, K. M., Yerkes, K. L., Michalak, T. E., Harris, R. J., and McQuillen, J., "Design of a Microgravity Spray Cooling Experiment," 42nd AIAA Aerospace Sciences Meeting and Exhibit, Reno, NV, AIAA Paper 2004-0966, 2004.

[57] Demiray, F., and Kim, J., "Microscale Heat Transfer Measurements During Pool Boiling of FC-72: Effect of Subcooling," *International Journal of Heat and Mass Transfer*, Vol. 47, Nos. 14–16, 2004, pp. 3257–3268. doi:10.1016/j.ijheatmasstransfer.2004.02.008